



Pergamon

Acta Materialia 50 (2002) 1349–1358



www.actamat-journals.com

Enhanced densification of zinc powders through thermal cycling

C.A. Schuh^{a, b, *}, D.C. Dunand^b

^a *Materials Science and Technology Division, Lawrence Livermore National Laboratory, Livermore, CA 94550, USA*

^b *Department of Materials Science and Engineering, Northwestern University, Evanston, IL 60208, USA*

Received 17 October 2001; received in revised form 21 November 2001; accepted 23 November 2001

Abstract

The densification of zinc powders by uniaxial hot pressing is investigated under both isothermal and thermal cycling conditions. Thermal cycling results in enhanced densification kinetics as compared to isothermal compaction at the upper cycle temperature. Using mechanistic models of initial-stage powder densification, the experimental data are analyzed to reveal the creep stress-exponent and activation energy of the dominant densification mechanism. Consequently, the observed densification enhancement during thermal cycling is confirmed to be due to internal stress plasticity, which is produced by internal mismatch stresses between adjacent zinc grains with anisotropic thermal expansion. © 2002 Acta Materialia Inc. Published by Elsevier Science Ltd. All rights reserved.

Keywords: Powder consolidation; Hot pressing; Zinc; Thermal expansion; Superplasticity

1. Introduction

During thermal cycling of bulk solids, many mechanisms can generate internal mismatch stresses, including (i) thermal expansion mismatch between phases in a composite, (ii) thermal expansion mismatch between grains in an anisotropic material, or (iii) solid-state phase transformation. Internal-stress plasticity (or internal-stress superplasticity), in which a small external applied stress is superimposed upon larger internal mismatch stresses, is an inherently stable deformation mechanism with an average stress exponent of

unity, arising from the biasing of the internal strains by the external applied stress [1,2]. In addition to a low stress-dependence of deformation, internal stress plasticity is characterized by rapid deformation rates, which are typically much higher than expected from the deformation mechanisms that would be active at the average temperature of the cycle (i.e. creep mechanisms). Although many additional sources of internal mismatch strain have been demonstrated (e.g. due to compressibility mismatch [3], radiation swelling [4], or chemical stresses [5,6]), internal stress plasticity is most commonly studied during thermal cycling. Recent reviews are available in [1,2] for the case of thermal expansion mismatch in composites and [1,7] for the case of phase transformation mismatch.

* Corresponding author. Fax: +1-925-422-6892.

E-mail address: schuh1@llnl.gov (C.A. Schuh).

Three materials with anisotropic coefficients of thermal expansion (CTE) have been shown to exhibit internal stress plasticity upon thermal cycling, including α -uranium [8], a magnesium alloy [9] and zinc [8,10–12]. In all of these studies, thermal cycling led to Newtonian flow in uniaxial loading (where the average strain rate during cycling, $\dot{\epsilon}$, or the strain increment developed after each thermal cycle, $\Delta\epsilon$, are proportional to the applied stress, σ), as compared to the fourth- or fifth-power law expected for typical creep deformation at the average temperature. Furthermore, superplastic tensile strains of $\sim 200\%$ without failure were reported by Wu et al. [10] upon multiple cycling of Zn under tension, due to necking inhibition associated with Newtonian flow.

Internal-stress plasticity has been modeled by many techniques and for many different specific cases of internal mismatch (e.g. [10,13–19]). However, only a few investigators have addressed the case of anisotropic CTE mismatch. The first to do so were Wu et al. [10], who assumed that the material deforms according to a hyperbolic-sine creep law, i.e. dislocation creep incorporating a power-law breakdown. They also assumed that thermal cycling induces a homogeneous internal stress σ_i due to the CTE mismatch between adjacent grains, and that this stress assists the motion of half of the dislocations in the specimen, and impedes the motion of the other half. Taking the two populations of dislocations to move independently, the authors derived a simple expression for the average creep rate during thermal cycling, which was predicted to be linear in the applied stress when $\sigma \ll \sigma_i$, in agreement with observations. Later, Zwigl and Dunand [18] presented a model for anisotropic CTE-mismatch internal stress plasticity, which was based on the successful model of Greenwood and Johnson [16] for deformation during an allotropic phase transformation. Noting mechanical similarity of these two types of internal-stress plasticity, Zwigl and Dunand replaced the transformation volume mismatch, $\Delta V/V$, with an effective internal volume mismatch due to anisotropic thermal expansion, assuming no texture in the specimen. Although this model was formulated for the case of time-independent yield under the combined stress state, the same approach

could be applied with a time-dependent model, as also considered by Greenwood and Johnson [16] and others for the case of transformation [20,21].

Both of the above models [10,18] predicted the observed linear flow law expected at low applied stresses, but the description of the internal stress state was approximate in each case, and the best quantitative agreement with experimental data are found by using the internal mismatch stress (or yield stress, in the case of Zwigl and Dunand [18]) as a fitting parameter. In contrast, the recent model of Kitazono et al. [12] uses a more rigorous micromechanical approach to describe the internal stress state in each grain, by considering a model spherical grain with a known orientation, embedded in a continuum matrix with average bulk properties. Considering the material to creep according to a power-law during triangular thermal cycles, these authors derived a closed-form expression for $\bar{\epsilon}$ that requires no fitting parameters, provided that the creep and thermal expansion properties of the material are known. By averaging over a known orientation distribution function, the effect of texture can also be considered quantitatively with this model. As with the previous models, the model of Kitazono et al. [12] predicts a linear flow law at low applied stresses.

Of the potential applications for internal-stress plasticity, one of continuing interest is the consolidation of powder aggregates, where this mechanism can lead to rapid densification at low stresses. Several studies have examined densification of metal powders during cyclic phase transformation [22–26], and noted significant increases in densification rate. In white cast-iron materials, the rapid low-temperature compaction due to internal-stress plasticity allowed the retention of a fine, metastable microstructure formed by rapid solidification [24]. In a recent study on consolidation of titanium powders [26], the operation of internal-stress plasticity was verified by quantitative analysis of the densification rate as a function of compact density and applied stress. This work also showed that, by adapting existing densification theories to the case of internal-stress plasticity, it is possible to identify the range of stress and relative density over which this mechanism dominates compaction kinetics [26]. Finally,

Daehn and co-workers [27–31], and others [32], have investigated compaction of composite powder blends during pressure cycling. Zavaliangos and Laptev [32] have emphasized the possibility of powder rearrangements during pressure cycling, while Jiang et al. [30] have conclusively demonstrated that the compressibility mismatch between stiff and compliant powder particles leads to internal-stress plasticity of the weaker powders, allowing faster consolidation and filling of small void spaces.

Despite the many studies described above, to our knowledge, there have been no investigations to date that consider powder compaction by internal stress plasticity for the case where mismatch strains are produced by anisotropic thermal expansion mismatch in single-phase materials. The purpose of the present work is thus to present experimental data on the initial-stage compaction of zinc powders, under both isothermal and thermal-cycling conditions. Additionally, we analyze the data with reference to existing densification theories, as well as the recent model of internal-stress plasticity due to Kitazono et al. [12], and present evidence for the operation of this mechanism during powder compaction.

2. Experimental procedures

The zinc powders used in this work were 99.9% pure, from Cerac (Milwaukee, WI), and were sieved to less than 150 μm and greater than 75 μm . Fig. 1(a) shows a scanning electron micrograph (acquired in a Hitachi S-4500 scanning electron microscope) of the powders, which exhibit an irregular shape with rounded edges, and an average aspect ratio near two. Each powder particle was polycrystalline, as revealed in the optical micrograph in Fig. 1(b) (etched with dilute HCl), with an average grain size $\sim 8 \mu\text{m}$.

Green powder compacts were obtained by cold pressing 7.57 \pm 0.10 g of powder in an aluminum die with a 12.70 mm bore diameter, using a double-action uniaxial press. The compacts were cold pressed under an applied pressure of 30 \pm 5 MPa to a relative density of $D_0 \equiv \rho/\rho_0 = 0.61 \pm 0.005$ (where ρ is the density of the compact and $\rho_0 =$

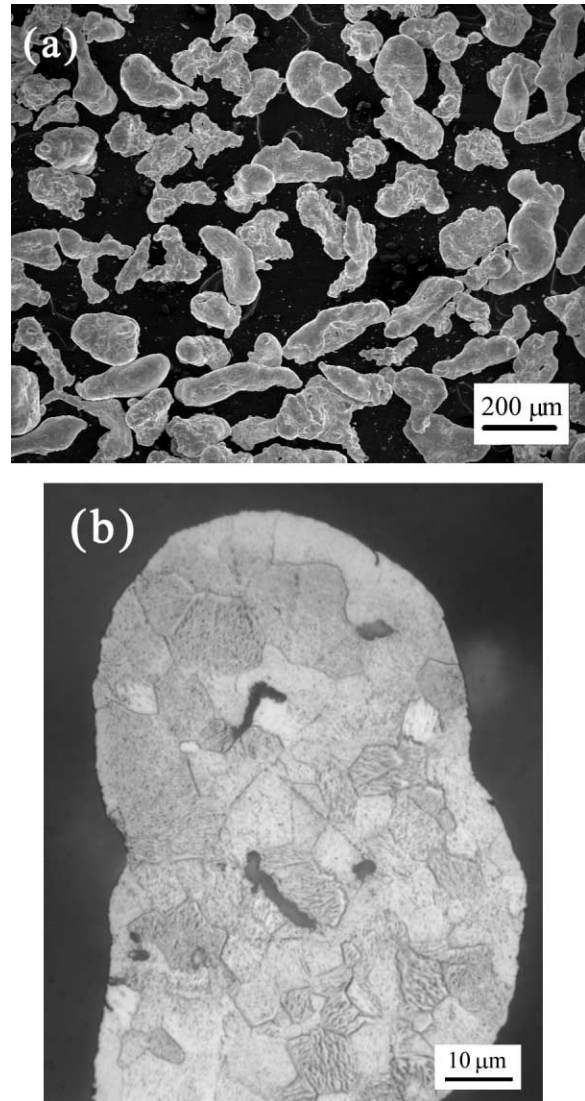


Fig. 1. As-received zinc powders observed by (a) scanning electron microscopy, showing the elongated shape of the powders, and (b) optical metallography, showing the grain size.

7.14 g/cm³ is the density of bulk zinc [33]). The green compacts were then placed in a cylindrical graphite die (12.71 mm bore diameter) for the hot-pressing experiments.

Hot pressing was performed in a radiant furnace described in [34], again in a uniaxial double-action geometry, with graphite punches. Temperature was monitored by a type-K thermocouple, which was in direct contact with the zinc powder compact

through a hole in the side of the cylindrical die. Two types of densification experiments were performed. First, isothermal densification experiments were undertaken at temperatures of 300 or 350 °C, under a nominal applied pressure $P_{\text{app}} = 3.60$ MPa. The length of the compact (from which its relative density was calculated) was measured continuously with a linear voltage-displacement transducer attached to the cold part of the load-train. Second, thermal-cycling densification was performed using a temperature amplitude of 200 K, and a cycle period of 6 min. For these experiments, the compact length was monitored only at the upper temperature of each thermal cycle to avoid errors introduced by thermal expansion and contraction of the load train. Using the same applied pressure $P_{\text{app}} = 3.60$ MPa, four experiments were completed with cycles in the ranges 75–275, 100–300, 125–325 and 150–350 °C; example thermal cycle profiles are shown in Fig. 2. Additionally, with a constant thermal cycle over the range 100–300 °C, three experiments were performed with $P_{\text{app}} = 1.15, 2.25, \text{ and } 3.60$ MPa.

Although the experiments were performed in air, the clearance between the punches and the die was sufficiently small to prevent significant oxidation

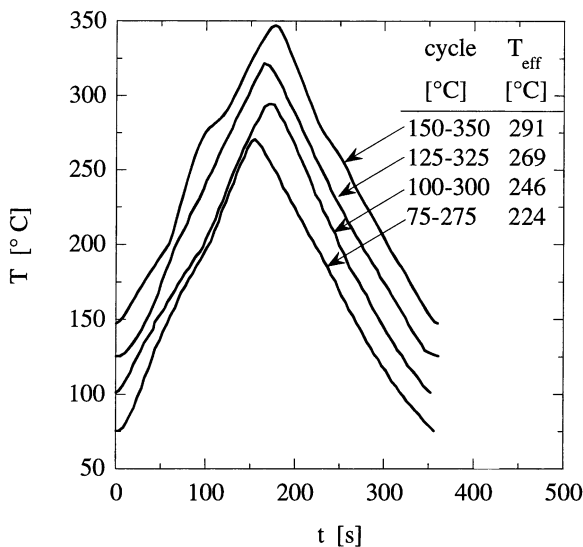


Fig. 2. Typical thermal cycle profiles used in compaction of zinc powders, and corresponding effective temperatures T_{eff} , as determined from Eq. (4).

of the powders; mass gain of the powder compacts after the experiments was invariably below 0.01 g (<0.1% change). To avoid trapping air in isolated pockets of the densifying compact, all of the experiments were terminated at densities below $D \sim 0.9$, corresponding to the transition from a compact with interconnected pores to a matrix with isolated voids. Thus, this investigation pertains only to the so-called initial stage of compaction [35].

3. Results

Fig. 3 shows the change in relative density of the zinc compacts during pressing at $P_{\text{app}} = 3.60$ MPa, for two isothermal and two thermal cycling experiments. Thermal cycling densification occurs much more quickly than isothermal compaction, despite the significantly lower average temperatures during thermal cycling. The effects of thermal cycle range (at constant pressure) and applied pressure (at constant thermal cycle range) on thermal-cycling densification are shown in Figs. 4 and

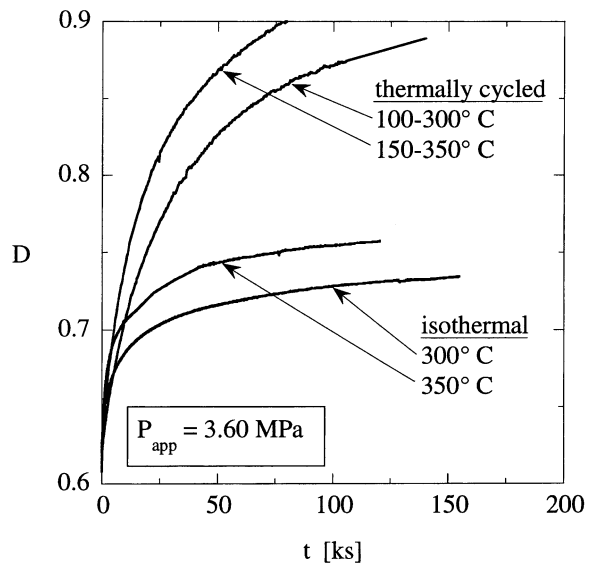


Fig. 3. Densification curves for an applied stress of 3.60 MPa and with temperature cycled over the ranges of 100–300 and 150–350 °C, showing enhanced densification as compared to isothermal tests at 300 and 350 °C.

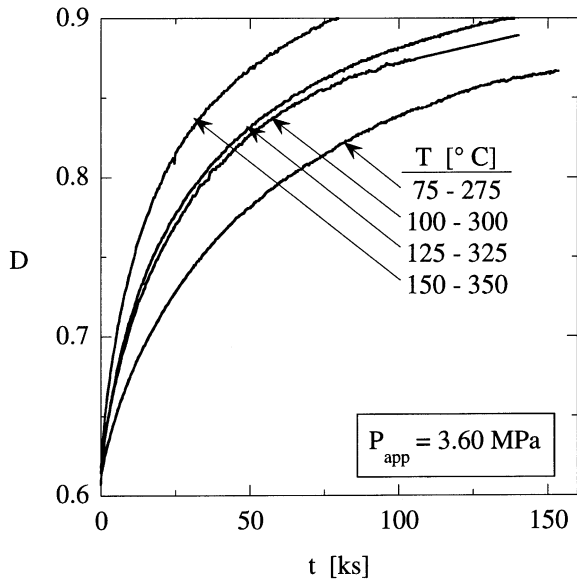


Fig. 4. Densification curves for various temperature ranges during thermal-cycling compaction at an applied stress of 3.60 MPa (with cycle profiles shown in Fig. 2).

5, respectively. As expected for any thermally-activated densification mechanism, densification rate increases with increasing temperature or applied pressure.

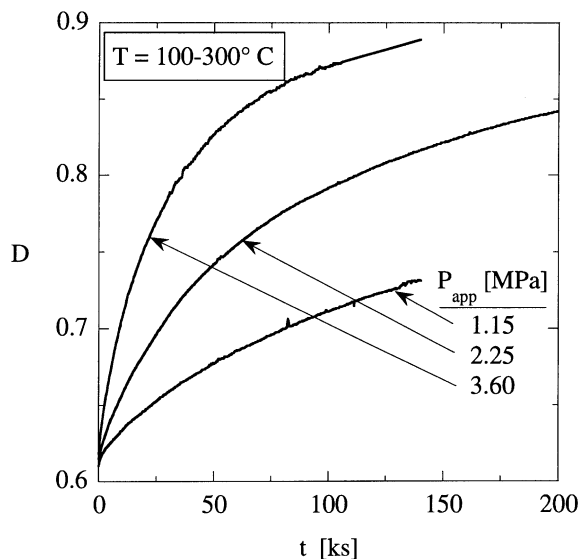


Fig. 5. Densification curves during thermal cycling over the range 100–300 °C at various applied uniaxial pressures, P_{app} .

The structure of a powder compact after densification at $P_{\text{app}} = 2.25$ MPa during thermal cycling over the range 100–300 °C is shown in Fig. 6. At a relative density of $D = 0.84$, the porosity appears to occur in generally isolated voids, although the interconnectivity of pores cannot be accurately judged from two-dimensional sections. Despite more than 55 h at elevated temperatures, the grain size for this specimen is still less than about 30 μm .

4. Discussion

The results in Fig. 3 unambiguously show that thermal cycling enhances the rate of compaction, even when compared to densification at the upper temperature of the cycle. We propose that this enhancement is due to the operation of internal-stress plasticity, activated by the thermal expansion mismatch between grains within each of the powder particles. In the sections to follow, we analyze the experimental results to elucidate the stress- and temperature-dependence of the dominant

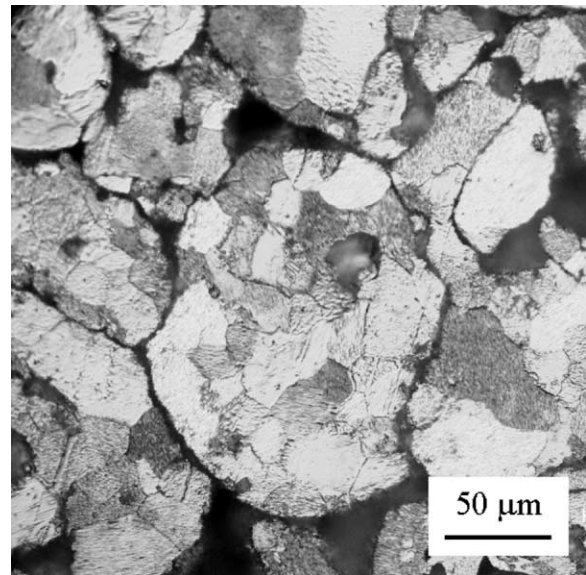


Fig. 6. Optical micrograph of a compact densified to $D = 0.84$ during thermal cycling over the range 100–300 °C, with $P_{\text{app}} = 2.25$ MPa.

densification mechanism, and thereby demonstrate the operation of internal-stress plasticity.

4.1. Mechanics of powder compaction

Although there are many approaches to modeling the densification of powders [36], the modeling approach of Arzt, Ashby et al. [35,37–41], as summarized by Helle et al. [35], represents a simple analytical framework which can be used to identify the dominant mechanism of densification, and which has been generally successful in describing various experimental densification data. Furthermore, while this approach was originally formulated for isostatic pressing of monosized spherical powders, it has been found to require little modification for uniaxial pressing [26,42–45]. Although the powders used in this investigation are non-spherical (Fig. 1), the expressions developed by Helle et al. [35] are still expected to capture the main dependencies of the densification rate on relative density, applied pressure, and temperature, thus allowing identification of the dominant mechanism of densification.

By considering the two-particle contact problem, as well as the increasing coordination of powder particles during densification, the effective pressure between powder particles is given by Helle et al. [35] as:

$$P_{\text{eff}} = P_{\text{app}} \frac{(1-D_0)}{D^2 \cdot (D-D_0)} \cdot B \quad (1)$$

where D_0 is the initial relative density of the compact prior to densification (taken as $D_0 \approx 0.62$ for closely-packed spheres [35]), and B is a constant introduced by Taylor et al. [45], which takes a value of unity for isostatic pressing, and is assigned a value of $B \approx 1.1$ for constrained uniaxial pressing [26]. Depending on the magnitude of P_{eff} and the test temperature, different densification mechanisms may operate, including diffusional transport, diffusional creep of the particles, or dislocation, power-law creep of the particles. For each of these mechanisms, Helle et al. [35] developed approximate, closed-form densification-rate expressions. For the present experiments on zinc performed at homologous temperatures between 0.50 and 0.90, densification is expected to

occur by a creep mechanism, according to a constitutive power-law:

$$\dot{\epsilon} = K \cdot \sigma^n \quad (2)$$

where $\dot{\epsilon}$ is the uniaxial steady-state creep rate, K is a temperature-dependent constant, σ is the uniaxial applied stress, and n is the stress-exponent of creep. Eq. (2), when generalized to three dimensions and applied to the two-particle problem, gives a form for the densification rate [35]:

$$\dot{D} = 3.06 \cdot (D^2 \cdot D_0)^{1/3} \cdot \left(\frac{D-D_0}{1-D_0} \right)^{1/2} \cdot K \cdot \left(\frac{P_{\text{eff}}}{3} \right)^n \quad (3)$$

For the case of zinc, power-law creep obeys Eq. (2) with a stress exponent $n \sim 4.5$ [10,12,46]. Internal stress plasticity, which occurs in bulk zinc during thermal cycling [10–12], follows a degenerate form of Eq. (2), where $n = 1$, and K is a function of the thermal profile, the thermal-expansion anisotropy, and the crystallographic texture of the material [12]. Thus, the main difference between these mechanisms is in the stress dependence, which can be determined from densification data according to Eq. (3), by plotting the quantity $\dot{D} \cdot D^{-2/3} \cdot (D-D_0)^{-1/2}$ against the effective pressure P_{eff} on double-logarithmic scales, and determining the stress exponent, n , from the slope of the data.

Such plots are shown in Fig. 7 for experiments with $P_{\text{app}} = 3.60$ MPa, comparing the densification during thermal cycling from 100–300 °C or 150–350 °C with isothermal densification at the respective upper cycle temperatures. Densification rates are found by calculating finite-difference derivatives of the raw densification data (from Fig. 3), and are assigned error bars of $\pm 50\%$, conservatively estimated from the scatter in the data. The effective pressure P_{eff} is calculated from Eq. (1); errors in this variable due to uncertainty in the measurement of D are very small. As shown in Fig. 7, thermal cycling leads to higher densification rates and considerably lower stress-dependence as compared to isothermal densification. Indeed, at least at higher values of P_{eff} , both of the thermal cycling data sets exhibit slopes close to unity (as expected for internal-stress plasticity, with $n = 1$ [12]), while the isothermal data sets have a much larger slope, near 4–5 (as expected for power-law creep, with $n \approx 4.5$ [46]). The possibility of dif-

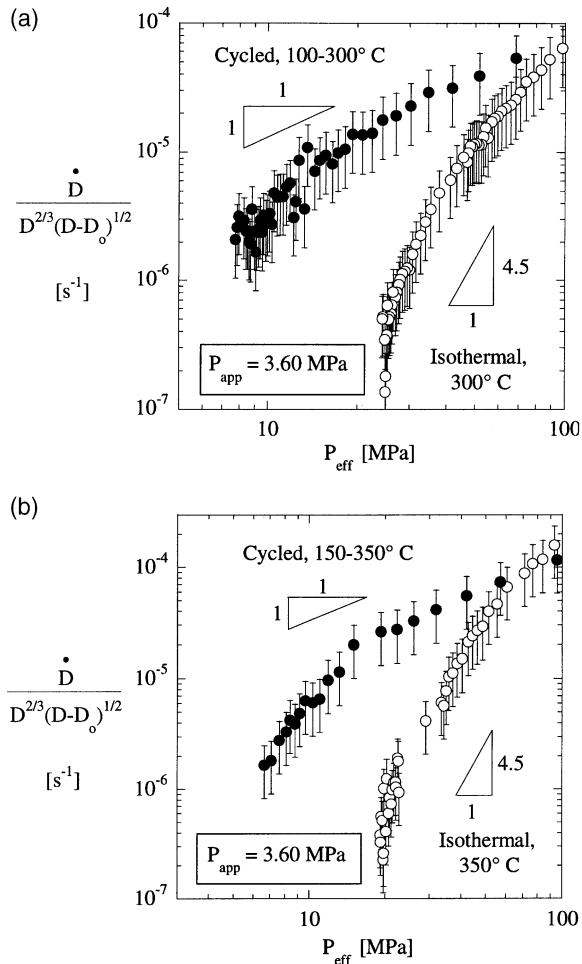


Fig. 7. Relative density-compensated densification rates, plotted against the effective contact pressure between particles for a constant applied stress of 3.60 MPa, for isothermal densification (a): 300 °C, (b): 350 °C and thermal-cycling densification (a): 100–300 °C, (b) 150–350 °C.

fusional creep during thermal cycling (also with $n = 1$) is ruled out, as this mechanism occurs at a lower rate than power-law creep, whereas the data in Fig. 7 show a clear increase in rate during cycling. Although only data from two thermal cycling experiments are shown in Fig. 7, similar trends are observed for all the other such experiments in Figs. 3–5.

The data plotted in Fig. 7 do not fall precisely onto lines of a single slope; there appears to be a consistent concave-downward curvature to all of

the data sets, for both isothermal and thermal cycling densification. This curvature is indicative of an additional density-dependence which is not considered by the model of Eqs. (1) and (3). If grains grow considerably during densification to sizes comparable to the powders, internal-stress plasticity cannot be assumed to occur within the bulk of each powder particle, and Eq. (3) with $n = 1$ cannot be used; rather, a micromechanical model considering single-crystal powders with anisotropic thermal expansion should be developed. However, comparing Fig. 1(b) and 6, it is apparent that only minor grain growth occurred during densification, so that the continuum approach [Eq. (3) with $n = 1$] can safely be used for the present experiments. A more likely explanation for the curvature in Fig. 7 is in the irregular shape of the powder particles (Fig. 1), which presents several deviations from the idealized mono-sized spherical unit-cell approximation made in the model. For example, increasing the aspect ratio of powder particles as a function of relative density, as well as the local curvatures and contact area between particles. Both of these effects would cause discrepancies between P_{eff} calculated from Eq. (1) and the true inter-particle stress. Additionally, particle shape changes might affect the transition from initial to final stage densification, which is identified with the closure of interconnected porosity into isolated voids. For spherical powders, this transition is usually taken to occur at $D = 0.90$ [35], but can begin as early as $D = 0.75$ [43]; for elongated particles, the transition may occur at even lower relative densities. As the structure of the compact diverges from initial to final stage densification, the geometrical assumptions behind Eqs. (1) and (3) no longer apply, and a linear slope is no longer expected in Fig. 7. The discrepancy between model and experiment is also highlighted by the magnitude of the interparticle stresses shown in Fig. 7. Typically, internal stress plasticity in zinc is more rapid than power law creep at stresses below about 2–20 MPa, depending on the cycle temperatures and frequency [10–12], whereas Fig. 7 suggests that internal stress plasticity is dominant below $P_{eff} \sim 60$ –100 MPa.

Despite the above sources of error, Fig. 7 shows

the expected qualitative trends of the model, and gives quantitatively reasonable values for the stress exponents. The low stress exponent near unity, combined with the higher rate of densification observed under thermal cycling conditions, represents strong evidence for the operation of transformation-mismatch plasticity as the dominant densification mechanism, although the quantitative values of P_{eff} are probably incorrect.

4.2. Temperature-dependence of thermal-cycling compaction

The linear stress dependence of internal stress plasticity described above is predicted by most all of the theoretical models of that phenomenon at low applied stresses [10,12,16,18]. However, the recent model of Kitazono et al. [12] highlights another important characteristic of this deformation mechanism—a weak temperature-dependence with a characteristic activation energy of Q/n_a , where Q and n_a are the activation energy and stress exponent of the mismatch-accommodation mechanism. For the case of power-law creep accommodation in zinc, $n_a \approx 4.5$, so the expected activation energy for internal-stress plasticity is less than one-quarter of that for creep.

Thermal cycles of different amplitude and duration are compared according to their effective temperatures, T_{eff} , at which the isothermal creep rate is an average over the thermal cycle. For symmetric, triangular thermal cycles, this is expressed as

$$\bar{\dot{\epsilon}}(T_{\text{eff}}) = \frac{1}{\Delta T} \int_{T_1}^{T_u} \dot{\epsilon}(T) dT \quad (4)$$

where T_u and T_1 are the upper and lower cycle temperatures, and $\Delta T = T_u - T_1$ is the cycle amplitude. For zinc, the temperature dependence of $\dot{\epsilon}$ is somewhat complicated; at temperatures below about 270 °C, the creep law is given by Eq. (2) with:

$$K = K' \cdot \exp\left(-\frac{Q}{RT}\right) \quad (5)$$

where $K' = 4.49 \cdot 10^{-22} \text{ Pa}^{-4.5} \text{ s}^{-1}$ and $Q = 91.7 \text{ kJ/mol}$, while above 270 °C, somewhat different

values of $K' = 8.93 \cdot 10^{-22} \text{ Pa}^{-4.5} \text{ s}^{-1}$ and $Q = 152 \text{ kJ/mol}$ apply [46]. In both temperature ranges, the power-law stress exponent is $n \approx 4.5$ [46]. The effective temperature of the approximately symmetric and triangular cycles used here is found by substituting Eqs. (2) and (5) into Eq. (4), using the appropriate values of K' and Q at each temperature during the cycle, and evaluating Eq. (4) numerically. The effective temperatures for the four thermal cycle profiles used in this work are shown in Fig. 2.

If densification occurs primarily due to a single thermally-activated mechanism, then the activation energy is related to the relative density and the densification rate through Eqs. (1–3) and (5), and the activation energy is found as the slope in plots of $\ln[\dot{D} \cdot D^{2n-2/3} \cdot (D-D_0)^{n-1/2}]$ vs $-1/T$. For the isothermal experiments performed in this work, $n \approx 4.5$, and the above relationship, evaluated between only two points (300 and 350 °C) gives an activation energy with very large error bars, $Q \sim 90 \pm 65 \text{ kJ/mol}$. The large uncertainty in this value results from the discrepancy between Eqs. (1) and (3) and the experimental data. As discussed previously, these equations appear to lack an additional density-dependent term when compared with the data; the Arrhenius relationship used to evaluate Q also lacks this density dependence, leading to uncertainty in the determined activation energy. Taking this error into account, and noting that this analysis is based on two data points which are only separated by 50 K in temperature, it is encouraging that the estimated range of activation energies encompasses the expected value of $Q \sim 152 \text{ kJ/mol}$ for dislocation creep at these temperatures [46].

The above Arrhenius relationship between density-compensated densification rate and $1/T$ cannot strictly be applied to the thermal cycling experiments, because all of the cycles cross the transition between two different activation energies, $Q = 91.7$ and 152 kJ/mol , which occurs at ~ 270 °C. However, these values of Q apply to the accommodation mechanism of internal stress plasticity (i.e. power-law creep); the actual activation energies for internal stress plasticity are expected to be $Q/n_a = 20$ and 34 kJ/mol , if cycling were to occur only below, or only above 270 °C, respectively [12].

Thus, the expected activation energy during cycling (20–34 kJ/mol) is significantly below that expected during isothermal creep (92–152 kJ/mol), and although the experimental data may exhibit scatter over these ranges, a simple Arrhenius analysis can readily distinguish which mechanism is responsible for densification during cycling.

Taking the stress exponent $n = 1$ for internal stress plasticity, the appropriate Arrhenius relationship ($\ln[\dot{D} \cdot D^{4/3} \cdot (D - D_0)^{1/2}]$ vs $1/T$, from Eqs. (1–3) and (5)) is plotted in Fig. 8 for the thermal cycling experiments performed with $P_{\text{app}} = 3.60$ MPa, according to the effective temperatures of the various thermal cycles given in Fig. 2; the data points represent average values over ranges of ~ 0.01 – 0.02 in D . As noted earlier for the case of isothermal compaction, the data points from a single experiment exhibit scatter over the value of $\dot{D} \cdot D^{4/3} \cdot (D - D_0)^{1/2}$, suggesting an additional density dependence that is not captured by this normalization. However, the scatter in the present case of thermal cycling is reasonable, and does not introduce a very large error on the determined acti-

vation energy of $Q = 33 \pm 10$ kJ/mol. As illustrated in Fig. 8, this activation energy is significantly lower than for isothermal creep, which occurs with $Q = 91.7$ – 152 kJ/mol. Furthermore, the value $Q = 33 \pm 10$ kJ/mol is within the range $Q = 20$ – 34 kJ/mol expected for internal stress plasticity, based on the model of Kitazono et al. [12]. This analysis further rules out densification by diffusional mass transport or diffusional creep, which would exhibit activation energies near that for either bulk ($Q = 152$ kJ/mol [46]) or grain-boundary diffusion ($Q = 60.5$ kJ/mol [46]).

5. Conclusions

Uniaxial hot-pressing experiments on zinc powders have shown that thermal cycling enhances the rate of densification, as compared to isothermal experiments at the upper cycle temperature. This enhancement is attributed to the operation of internal stress plasticity, which is a rapid Newtonian deformation mechanism that arises when internal and external stresses are superimposed. In the present experiments, the anisotropic thermal expansion of zinc leads to internal stress generation between adjacent grains within the powders, and the applied compaction pressure provides a biasing stress for more rapid densification.

Using mechanistic models of powder densification, the experimental data have been analyzed to determine the stress- and temperature-dependence of the dominant densification mechanisms. In isothermal experiments, a stress exponent of $n \approx 4.5$ is observed, which is consistent with the power-law creep mechanism for pure zinc. In contrast, during thermal cycling, a much weaker stress dependence is observed, with a power-law exponent near unity, as expected for internal stress plasticity. Additionally, the activation energy for densification during thermal cycling $Q \sim 33$ kJ/mol is very low compared to that for power-law creep or bulk diffusion, $Q = 92$ – 152 kJ/mol, and is in line with the expected value for internal stress plasticity of zinc, $Q/n = 20$ – 34 kJ/mol.

The combined observations of (i) enhanced densification during thermal cycling, (ii) a low stress-exponent near unity and (iii) an anomalously

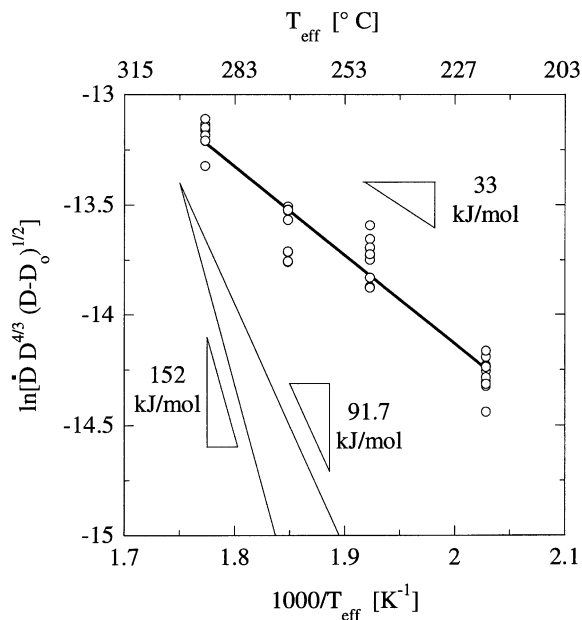


Fig. 8. Arrhenius plot of relative density-compensated densification rate against reciprocal effective temperature (listed in Fig. 2), for thermal cycling experiments with an applied stress of 3.60 MPa.

low activation energy, confirm the operation of internal stress plasticity during initial stage powder compaction in zinc. To our knowledge, this is the first report of internal stress plasticity in a powder compaction process, in which thermal expansion mismatch generates the internal stress state. We expect this mechanism to be active during densification of other types of powders with thermal expansion mismatch, including metal or ceramic powders with anisotropic thermal expansion (e.g. α -U or ZrO_2) or blends of two or more powders with different thermal expansion (e.g. Cu/W, Al/SiC or $\text{Al}_2\text{O}_3/\text{ZrO}_2$).

Acknowledgements

This study was supported by the National Science Foundation through grant DMR-9987593. C.S. additionally acknowledges the support of the University of California, Lawrence Livermore National Laboratory, under US Department of Energy contract No. W-7405-Eng-48.

References

- [1] Nieh TG, Wadsworth J, Sherby OD. Superplasticity in metals and ceramics. Cambridge: Cambridge University Press, 1997.
- [2] Clyne TW, Withers PJ. An introduction to metal matrix composites. Cambridge: Cambridge University Press, 1993.
- [3] Huang CY, Daehn GS. In: Ghosh AK, Bieler TR, editors. Superplasticity and superplastic forming 1995. Warrendale, PA: TMS; 1996:135.
- [4] Roberts AC, Cottrell AH. *Phil Mag* 1956;1:711.
- [5] Frary M, Schuh C, Dunand DC. *Phil Mag A* 2001;81:197.
- [6] Dunand DC, Zwigl P. *Metall Mater Trans A* 2001;32:841.
- [7] Dunand DC. In: Chandra T, Sakai T, editors. International Conference on Thermomechanical Processing of Steels and other Materials. Warrendale, PA: TMS; 1997:1821.
- [8] Lobb RC, Sykes EC, Johnson RH. *Met Sci J* 1972;6:33.
- [9] Kitazono K, Sato E, Kuribayashi K. *Scripta Mater* 2001;44:2695.
- [10] Wu MY, Wadsworth J, Sherby OD. *Metall Trans A* 1987;18:451.
- [11] Pickard SM, Derby B. *Scripta Metall Mater* 1991;25:467.
- [12] Kitazono K, Hirasaka R, Sato E, Kuribayashi K, Motegi T. *Acta Mater* 2001;49:473.
- [13] Daehn GS, Xin XJ, Wagoner RH. In: Earthman JC, Mohamed FA, editors. Creep and fracture of engineering materials and structures. Warrendale, PA: TMS; 1997, p. 257.
- [14] Daehn GS, Zhang H, Chen YC, Wagoner RH. In: Lowe TC, Rollet T, Follansbee P, Daehn GS, editors. Modeling the deformation of crystalline solids. Warrendale, PA: TMS; 1991:665.
- [15] Daehn GS, Gonzalez-Doncel G. *Metall Trans A* 1989;20:2355.
- [16] Greenwood GW, Johnson RH. *Proc Roy Soc Lond A* 1965;283:403.
- [17] Poirier JP. *J Geophys Res* 1982;87:6791.
- [18] Zwigl P, Dunand DC. *Acta Mater* 1997;45:5285.
- [19] Zwigl P, Dunand DC. *Mater Sci Eng A* 1999;262:166.
- [20] Mitter W. Umwandlungsplastizität und ihre Berücksichtigung bei der Berechnung von Eigenspannungen. Berlin: Gebr. Bornträger, 1987.
- [21] Schuh C, Dunand DC. *Acta Mater* 2001;49:199.
- [22] Kohara S. *Metall Trans A* 1976;7:1239.
- [23] Oshida Y. *Jpn Soc Powder Metall* 1975;22:147.
- [24] Ruano OA, Wadsworth J, Sherby OD. *Metall Trans A* 1982;13:355.
- [25] Leriche D, Gautier E, Simon A. In: Sixth World Conference on Titanium, 1988:1295.
- [26] Schuh C, Noel P, Dunand DC. *Acta Mater* 2000;48:1639.
- [27] Huang CY, Daehn GS. *Acta Mater* 1996;44:1035.
- [28] Huang C-Y, Daehn GS. *Acta Mater* 1997;45:4283.
- [29] Jiang G, Wu W, Daehn GS, Wagoner RH. *Acta Mater* 2000;48:4331.
- [30] Jiang G, Daehn GS, Wagoner RH. *Scripta Mater* 2001;44:287.
- [31] Jiang G, Daehn GS, Wagoner RH. *Scripta Mater* 2001;44:1117.
- [32] Zavaliangos A, Laptev A. *Acta Mater* 2000;48:2565.
- [33] Brandes EA, Brook GB, editors. *Smithells metals reference book*. Oxford: Butterworth-Heinemann; 1999.
- [34] Schuh C, Han BQ, Dunand DC. *Metall Mater Trans A* 2000;31:2647.
- [35] Helle AS, Easterling KE, Ashby MF. *Acta Metall* 1985;33:2163.
- [36] German RM. *Powder metallurgy science*. Princeton, NJ: Metal Powder Industries Federation, 1994.
- [37] Wilkinson DS, Ashby MF. *Acta Metall* 1975;23:1277.
- [38] Wilkinson DS, Ashby MF. In: Kuczynski GC, editor. 4th International Conference on Sintering and Related Phenomena. New York: Plenum Press; 1975. p. 473.
- [39] Arzt E. *Acta Metall* 1982;30:1883.
- [40] Arzt E, Ashby MF, Easterling KE. *Metall Trans A* 1983;14:211.
- [41] Fischmeister HF, Arzt E. *Powder Metall* 1983;26:82.
- [42] Ogbonna N, Fleck NA. *Acta Metall Mater* 1995;43:603.
- [43] Fleck NA, Kuhn LT, McMeeking RM. *J Mech Phys Solids* 1992;40:1139.
- [44] Sridhar I, Fleck NA. *Acta Mater* 2000;48:3341.
- [45] Taylor N, Dunand DC, Mortensen A. *Acta Metall Mater* 1993;41:955.
- [46] Frost HJ, Ashby MF. *Deformation-mechanism maps: the plasticity and creep of metals and ceramics*. Oxford: Pergamon Press, 1982.